Graphene oxide framework membranes intercalated by poly(sodium 4-styrenesulfonate) for efficient desalination

Hui Xu, Jincheng Huang, Hong Qi *

College of Chemical Engineering, Nanjing Tech University, Nanjing 210009, China

* Tel. +86-25-83172279; Email: hqi@njtech.edu.cn

Abstract

GO membranes with well-defined sub-nanometer channels are optimal for desalination and wastewater purification. However, the inherent instability of the interlayer structure and the severe trade-off between selectivity and permeability pose a significant challenge for GO membranes to be effectively applied to nanofiltration. Herein, we synthesized a series of PSSNa-GO-EDA/Al_2O_3 membranes by embedding poly(sodium 4-styrenesulfonate) (PSSNa) into ethylenediamine-crosslinked GO interlayers. The resultant membranes exhibited greater interlayer structures, in which new hydrophilic confined nanostructures were constructed. Effective nanofiltration performance was achieved through electrostatic-induced ion-confined partitioning. The PSSNa-GO-EDA-1/Al_2O_3 (PGE-1) membrane showed high rejection rates of 86.0% for Na_2SO_4 and 53.8% for NaCl while maintaining competitive pure water permeance of 10.85 LMH/bar, which is 12.1 times higher than that of the pristine GO membrane. More importantly, after immersion in pure water for 680 hours, this membrane retained commendable separation performance. Overall, our work provides an effective strategy to finely fabricate confined nanostructures in lamellar GO-based nanofiltration membranes featuring excellent separation performance.

Keywords: Graphene oxide membrane; PSSNa; Confined nanostructures; Desalination

1. Introduction

Owing to accelerated industrialization, population expansion, and freshwater pollution, the scarcity of clean water has emerged as one of the greatest humanitarian crises worldwide[1, 2]. To solve the issue of water scarcity, a range of separation and purification technologies have been developed. In contrast to traditional purification techniques such as distillation and electrodialysis, membrane separation technology has demonstrated excellent application prospects due to its benefits of lower energy consumption, higher efficiency, and eco-friendliness [3-5].

Graphene oxide, a kind of novel two-dimensional material, has drawn significant attention due to its atomic thickness, outstanding physicochemical properties, and easily functionalized surface characteristics[6-9]. Additionally, self-supported GO membranes could be directly synthesized through the stacking of GO nanosheets[10]. Nevertheless, the self-supported GO membrane faces numerous difficulties in practical applications. Simultaneously, on account of its swelling property, it is difficult for the GO membrane to ensure the stability of the laminar structure in water [11, 12]. Even more seriously, the laminar GO membranes possess tortuous, narrow, and lengthy transport channels, which have high solute rejection rates but are often accompanied by extremely low water permeability. This situation severely restricts the application of GO membranes due to the selectivity-permeability trade-off[13, 14].

In response to the challenges in the applications of GO membranes, numerous methods have been developed over the past two decades[15, 16], such as physical confinement, thermal or chemical reduction, and cross-linking. For example, Abraham et al. [17] achieved the adjustment of the interlayer distance of laminar GO membranes from 9.8 Å to 6.4 Å by employing epoxy resin for encapsulation. On the other hand, an extensive array of crosslinkers with diverse chemical properties and functionalities has been extensively employed to overcome the swelling of GO membranes. Molecules or polymers containing amine groups are regarded as ideal crosslinkers for GO membranes, such as polydopamine [18], polyethyleneimine[19], amino acids[20], ginger plant extractive[21], and ethylenediamine[22]. For instance, Jin et al. [23] put forward a method of constructing "molecular bridges" which they rationally built and tuned to stabilize the GO membranes. The molecular-bridged GO membranes demonstrated exceptional durability under severe operating conditions. Consequently, the molecular-bridged GO membranes had an outstanding dye removal rate of over 99%. Its ion rejection, however, was not satisfactory.

Naturally, the covalent or non-covalent cross-linking method is not limited to the application of a single cross-linker but is also widely employed for double cross-linkers [24, 25]. For example, Xu et al. [26] used metal-polyphenol double-crosslinked GO membranes for dye/salt separation. Their results indicated that the membrane not only showed a larger interlayer spacing and superior hydrophilicity, but its surface negative charge also exhibited a decreasing tendency. Hence, the membranes exhibited an exceptional removal rate for organic dyes, reaching 99% or more, and a high permeability of 61.2 LMH/bar.

For two-dimensional laminar GO membranes, regulating the interlayer distance and modifying the surface chemical characteristics or interlayer can be effective ways to achieve excellent separation performance. Shao et al. [27]designed a novel coordination complex as the modifier to fabricate hydrophilic GO membranes. The interaction between the Fe^{3+}-phytic acid coordination complex and the GO nanosheets modulated the interlayer distance of the GO membranes. As a result, this complex enhanced the hydrophilic characteristics of GO membrane surfaces, improved the composite membrane's water sorption capacity and facilitated rapid water transport. Moreover, Dai et al. [28] stabilized the stacked laminar GO membrane structure by introducing sodium polystyrene sulfonate into the interlayer of the GO membrane. Due to the exceptional properties of the sulfonic acid groups, the modified structure is both hydrophilic and charged in the interlayer structure, providing a favorable hydrophilic microenvironment to facilitate selective water molecule transport. Their results revealed that the PSSNa/GO membrane fabricated with this strategy demonstrates exceptional pervaporation separation properties.

Therefore, the enhancement of the stability of the laminar structure of GO membranes, coupled with the establishment of chemically distinct environments or microregions with specialized confinement functions on the surface or within the interlayers, represents a pivotal strategy for optimizing the performance of lamellar GO membranes in water.

In this paper, we incorporated sodium polystyrene sulfonate into the amine-crosslinked GO membrane interlayer and deposited GO-based nanosheets onto the inner tube ceramic membranes via the pressure-assisted deposition approach. The resultant GO composite ceramic nanofiltration membranes were prepared as depicted in Fig. 1. We have developed a new approach to creating hydrophilic confined nanostructures within the interlayer of GO membranes. This method has the potential to stabilize the laminar structures of these membranes and increase interlayer spacing, which could enhance pure water permeability. Additionally, it may be effective in confining ions in saline solutions via ion electrostatic induction forces. This mechanism significantly mitigates the synergistic transport effects between cations and anions, thereby improving rejection rates. The results demonstrate that the PSSNa-GO-EDA-1/Al_2O_3 (PGE-1) membrane achieves rejection rates of 86.0% for Na_2SO_4 and 56.4% for NaCl while maintaining competitive water permeability of 10.85 LMH/bar (12.1-fold higher than that of pristine GO membrane). Moreover, the PSSNa-GO-EDA-1/Al_2O_3 membrane demonstrates outstanding stability during long-term filtration processes. Thus, we are confident that this approach will significantly enhance practical applications of GO membranes in water purification.

2. Experimental

2.1. Materials

GO nanosheets (lateral size: 500–5000 nm, 1 mg·mL^{-1}, XFNANO), Tris (hydroxymethyl) aminomethane hydrochloride (Tris-HCl, 99%, Aladdin), Hydrochloric acid (HCl, 36wt%, Lingfeng)， poly(sodium 4-styrenesulfonate) (PSSNa, MW=70000, 99%, Aladdin), Anhydrous ethylenediamine (EDA, 99%, Adamas), Na_2SO_4, NaCl, $MgSO_4$, and $MgCl_2$ (99%, Lingfeng), Dopamine hydrochloride (98%, Aladdin) were used without additional purification. 110-mm-long tubular Al_2O_3 ceramic membranes with inner and outer diameters of 8 and 12 mm (pore size: 20 nm) were obtained from Hongyi (Nanjing, China).

2.2 Preparation of PDA- pre-treated tubular Al_2O_3 ceramic membranes

First of all, 2 mg/ml aqueous solution of dopamine hydrochloride was mixed with 10 mM Tris-HCl solution stirring at 25 °C. After thoroughly mixing the solution, the tubular Al_2O_3 membranes were subsequently treated with this solution at 25 °C for 20 hours to promote the self-polymerization of polydopamine in a dark environment. Following this, the membranes were rinsed with pure water to remove any residual dopamine from the inner surface of the tubular Al_2O_3 membranes. Finally, the tubular ceramic membranes were dried in an electric-heated constant-temperature air-circulating drying oven at 60 °C for two hours to obtain polydopamine-modified Al_2O_3 membranes, hereafter referred to as the PDA-Al_2O_3 membranes.

2.3 Preparation of pristine GO and GO-based membranes

First, 0.2 ml of GO dispersion was diluted to 200 ml with pure water, and the single-layer GO nanosheets were completely dispersed in the 200 ml dilution by sonication for 10 min. After that, to prepare the GO-EDA (GE) suspension, 13.5 μL of EDA was added to the GO solution. After thoroughly mixing the solution, the mixture was stirred at 80 °C for 60 min. Subsequently, the prepared GE suspension was mixed with a specific quantity of sodium polystyrene sulfonate aqueous solution and sonicated for 15 minutes to form a homogeneous PSSNa-GO-EDA (PGE)solution.

The suspensions with different amounts of PSSNa were loaded onto the internal surface of the prepared PDA-Al_2O_3 membrane under pressurized nitrogen at 1 bar. Finally, the fabricated membranes were dried at 45 °C overnight in an electric-heated constant-temperature air-circulating drying oven to obtain PSSNa-GO-EDA/Al_2O_3

membranes. The resulting PSSNa-GO-EDA/Al_2O_3 membranes were labeled PGE-*x* (*x* = 1, 2, 3). The theoretical mass ratios of GO and PSSNa are 1:150, 1:250, and 1:400, and the composite membranes are named PGE-1, PGE-2, and PGE-3, respectively. Pristine GO and GO-EDA membranes were fabricated following the same strategy, except that EDA and PSSNa were not added. The preparation process of the PGE membranes is illustrated in Fig. 1.

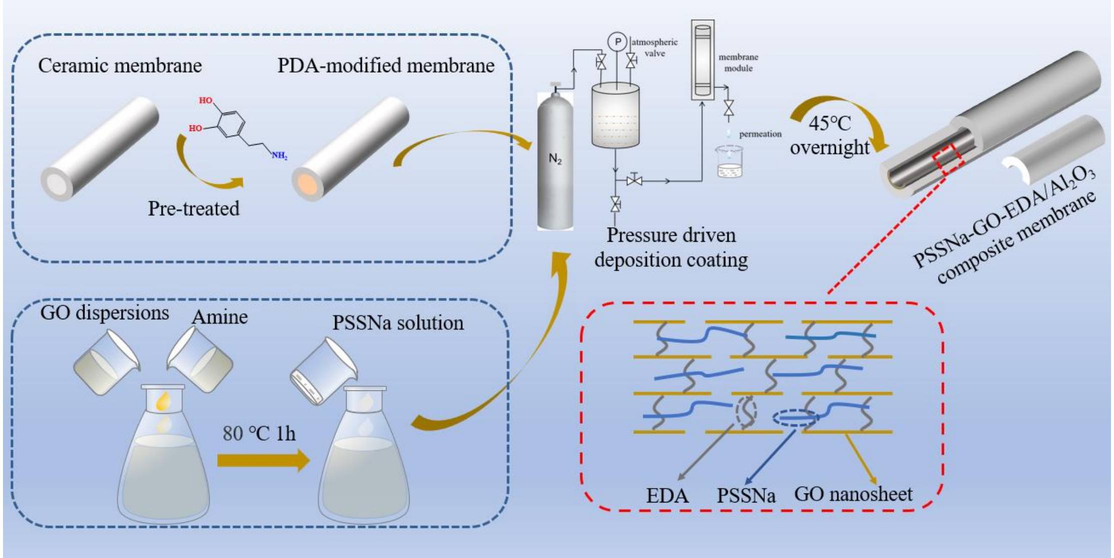

Fig. 1. Schematic diagram of the preparation processes of PGE membranes

2.4 Characterizations of GO and GO-based membranes

Zeta potential of the prepared membrane samples was tested by Zetasizer analyzer (Nano ZS-90). Fourier transform infrared spectrometer (FT-IR, Nicolet 8700), X-ray photoelectron spectroscopy (XPS, Al Kα, ESCALAB 250), X-ray diffraction (XRD, Cu Kα, Mini Flex 600), and Scanning electron microscopy (SEM, Sigma 360) were performed to investigate the chemical composition, the interlayer structure and the morphologies of the prepared membrane samples, respectively. The contact angles (CA) of the prepared membrane samples were measured using a contact angle tester (Drop Meter A-100P).

2.5 Evaluation of the membrane performance

The prepared membrane separation performance was evaluated using 1 mM single-component salt solutions (Na_2SO_4, $MgSO_4$, NaCl, $MgCl_2$) under 5 bar on a self-built cross-flow filtration device at 25 °C. The stability of the GO-based membranes was tested through a long-term water immersion test. The pure water permeance of GO-based membranes were tested continuously for 4 h. The salt rejection performance test was conducted after the system was stabilized for 40 minutes. Subsequently, to ensure data accuracy, the permeate was collected at 5-minute intervals for a total of four collections.

After soaking the GO-based membranes in pure water for different periods of time (170 h, 340 h, 510 h, and 680 h), the rejection of the above four single-component salt solutions was measured under the corresponding soaking time. The pure water permeance J (LMH/bar) and the salt rejection R are calculated with the following equations:

$$J = \frac{V}{At\Delta P} \tag{1}$$

$$R = (1 - \frac{C_p}{C_f}) \times 100\% \tag{2}$$

where V (L) is the volume of permeate; A (m^2) is the effective membrane area; t (h) is permeation time; ΔP (bar) is the operating pressure. C_f and C_p are the feed and permeate concentrations of salt solutions.

3. Results and discussion

3.1 Performance of the PDA-Al_2O_3 tubular membrane

The morphologies of Al_2O_3 and PDA-Al_2O_3 membranes were analyzed using SEM. As shown in Fig. 2, the alumina particles are evenly dispersed on the surface of the Al_2O_3 membrane, and the surface of PDA-Al_2O_3 membrane is obviously covered with a material layer. It is also evident from the optical images that the membrane surface turns black following PDA modification. From Fig. 2b, d, the PDA is closely covered on the Al_2O_3 membrane without obvious boundary. The pure water flux of the Al_2O_3 and PDA-Al_2O_3 membranes was evaluated. It can be seen from Fig. 3 that the modified membrane exhibits a 20.8% reduction in pure water permeance (82.8 LMH/bar) compared with that before modification. Furthermore, the rejection rates of the Al_2O_3 and PDA-Al_2O_3 membranes for the four salt solutions are all below the detection limit of the conductivity meter (the rejection rates can be regarded as zero). The results indicate that PDA was successfully grafted on the Al_2O_3 membrane via self-polymerization[29].

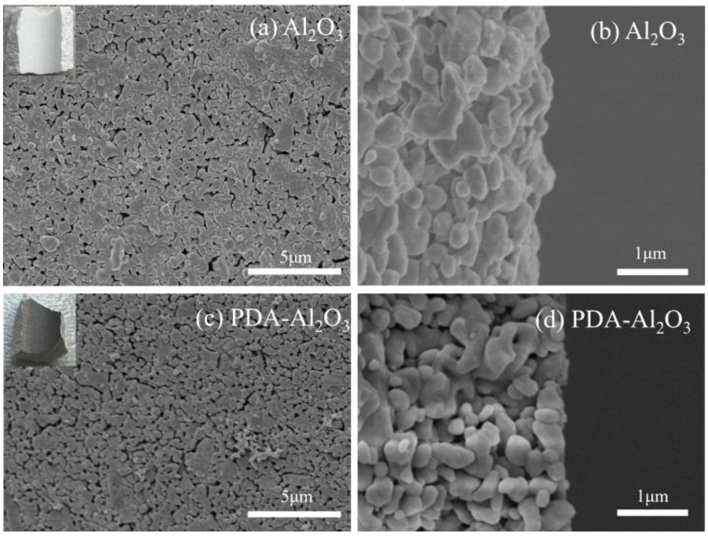

Fig. 2. SEM images of (a, c) surfaces, (b, d) cross-sections of the Al_2O_3 and PDA-Al_2O_3 membranes

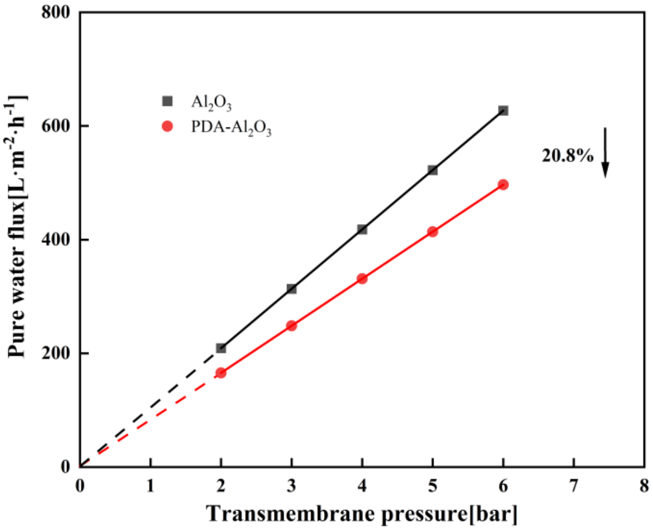

Fig. 3. Pure water flux of Al_2O_3 and PDA-Al_2O_3 tubular membranes

3.2 Characterizations of GO-based membranes

The well-dispersible GO suspension constitutes a prerequisite for preparing separation membranes with excellent performance. As shown in Fig. 4, the zeta potential of the five membrane-forming suspensions is all negative, and the lowest zeta potential is witnessed in the PGE-1. This is attributed to the abundant negatively charged ionized sulfonic acid groups in PSSNa, which gives rise to a reduction in the zeta potential of the suspensions containing PSSNa. The lower the zeta potential is, the better the dispersibility of the suspension becomes. This is conducive to depositing nanosheets on the tubular ceramic membrane in preparing GO-based separation membranes with good laminar structure.

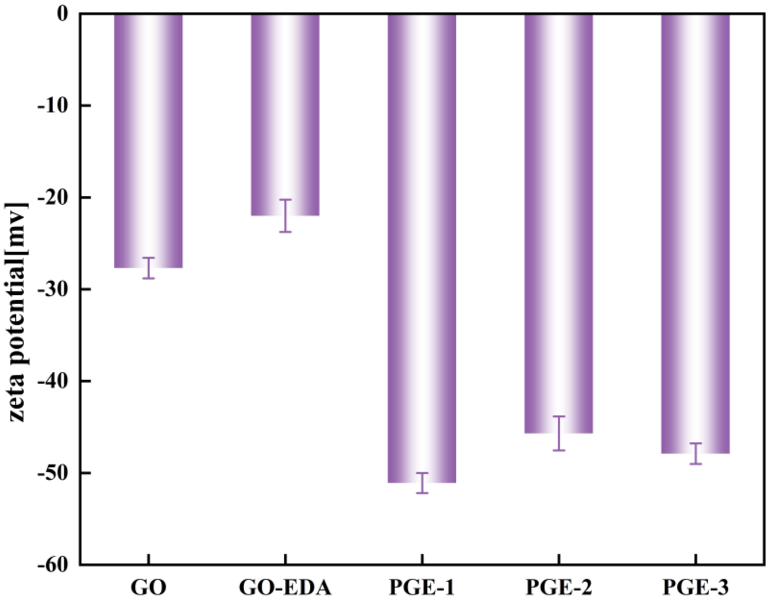

Fig. 4. Zeta potential of pristine GO, GE, PGE membrane-forming suspension

Fig. 5 shows the FTIR spectra of PSSNa, pristine GO, GE, and PGE membranes; the characteristic peaks of the pristine GO membrane located at ~3443, ~1729, ~1625, ~1406, and ~1226 cm^{-1} were assigned to -OH, C=O, C=C, C-OH, and C-O-C, respectively. These values are in agreement with the previous report [30]. When the GO nanosheets were crosslinked with EDA, the characteristic peaks of carboxyl and epoxy groups were no longer observed due to the existence of EDA [31]. Besides, there are two peaks at ~1583 and ~1481 cm^{-1}, which can be attributed to amine (N-H) and amide (C-N) respectively [32]. This occurs due to the covalent reaction of the amine groups in EDA with the oxygenated groups on the GO laminar nanosheets[33], thus proving the successful introduction of EDA into the GO membranes. For PGE membranes, there are two additional distinct peaks located at ~1129 and ~1191 cm^{-1}[28]. These peaks indicate the stretching vibration of S=O of -SO_3^-, which substantiates the incorporation of PSSNa into the two-dimensional interlayer channel of GO-based membranes. Furthermore, the XPS full-spectrum in Fig. 6 shows that the novel peaks at 400 eV were identified in both GE and PGE membranes, corresponding to the N1s convolution peak[31]. Meanwhile, new peaks at 168 eV were detected in the PGE membranes. Further fitting of the S 2p curve reveals that the two additional distinct peaks at 167.8 eV and 169.0 eV represent the oxidized sulfur in the -SO_3^-, which was attached to the benzene structure within PSSNa[28, 34]. These findings demonstrate that EDA and PSSNa have effectively introduced two-dimensional interlayer channels into GO membranes.

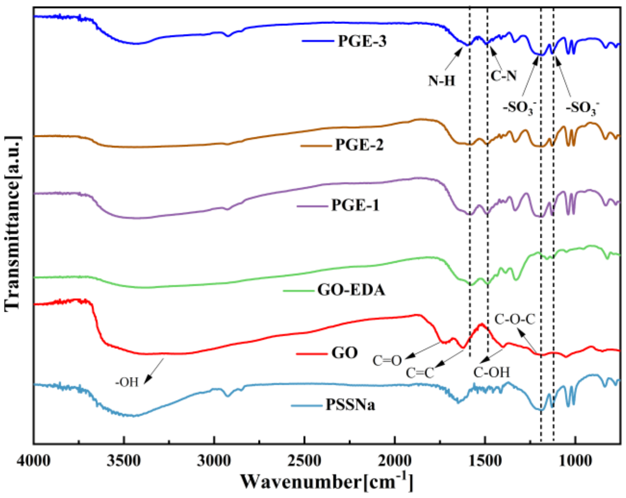

Fig. 5. FTIR spectra of PSSNa, GO, GE, and PGE membranes

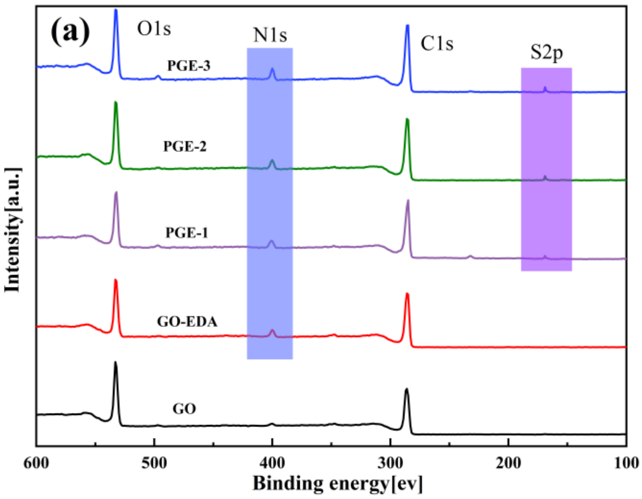

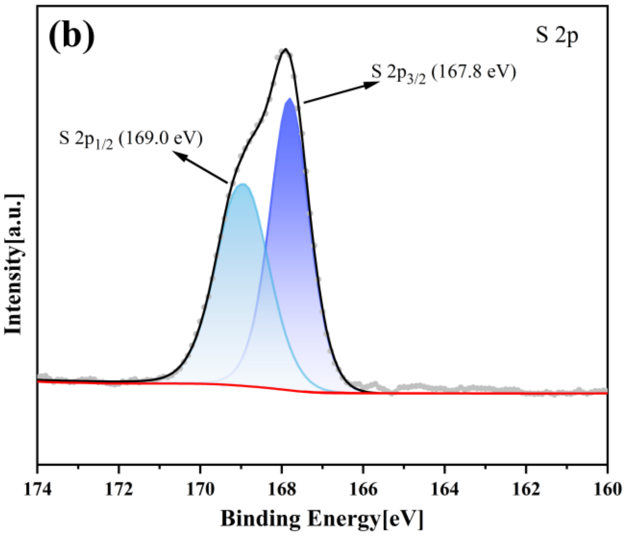

Fig. 6. (a) XPS full-scan spectra of GO, GE, and PGE membranes; (b) S 2p spectra of PGE-1 membrane

For lamellar separation membranes, a complete and defect-free membrane structure is of crucial significance for their application. As shown in Fig. 7, the surfaces of the GO, GE, and PGE membranes are smooth and continuous, and all of them possess typical wrinkles, suggesting that the GO-based membranes have been successfully coated onto the tubular ceramic support. Furthermore, the thickness of the pristine GO membrane layer was 72 nm according to Fig. 7(a2), while those of the GE, PGE-1, PGE-2, and PGE-3 membranes increased to 86, 152, 183, and 205 nm, respectively, with the intercalation of EDA and PSSNa into the interlayer structure. Additionally, all five membranes maintain excellent interlayer structures.

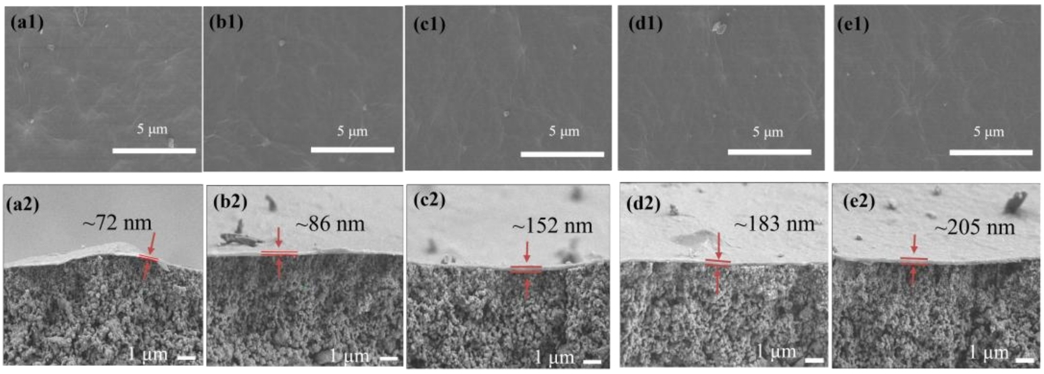

Fig. 7. SEM images of (a1) GO, (b1) GE, (c1) PGE-1, (d1) PGE-2, (e1) PGE-3 membrane surfaces and (a2) GO, (b2) GE, (c2) PGE-1, (d2) PGE-2, (e2) PGE-3 membrane cross-sections

Normally, water molecules exposed to the membrane surface will be absorbed into the membrane by the chemical potential difference [35, 36]. Consequently, as the membrane layer becomes more hydrophilic, water molecules are able to penetrate the membrane more readily. Therefore, to evaluate the hydrophilicity of the membrane, we measured the water contact angle (WCA) of the GO, GE, and PGE membranes. As illustrated in Fig. 8, the WCA of the pristine GO membrane is 57.8°; this finding is in agreement with the results presented in the prior study [33] and indicates that the membrane is of a hydrophilic nature. With the crosslinking of EDA, the WCA of the GE membrane reduced, as the diamine groups crosslinked on the GE membrane layer are hydrophilic and prone to forming hydrophilic regions. This effect could enhance the hydrophilicity of the GE membrane layer[32, 33]. For the PGE-1, PGE-2, and PGE-3 membrane, the WCA decreased from 44.7° to 37.3°. PSSNa contains a significant number of hydrophilic sulfonic acid groups, and incorporating PSSNa into lamellar GO membranes can enhance the ability of PGE membranes to attract water molecules.

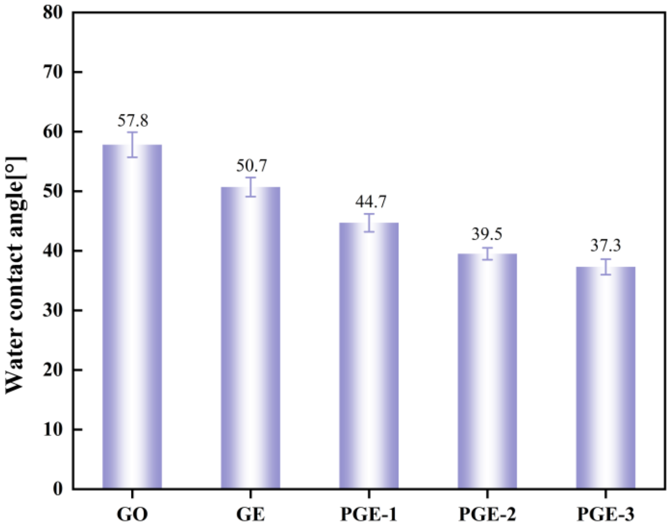

Fig. 8. WCA of GO, GE, and PGE membranes

The laminar interlayer structures of the GO, GE, and PGE membranes were analyzed by XRD. Fig. 9 presents the XRD patterns of GO, GE, and PGE membranes. There is a diffraction peak at 11.02° for the pristine GO membrane, corresponding to an interlayer spacing of 0.803 nm. This is consistent with the previous literature[37]. For the GE membrane, the diffraction peak shifts to a lower angle (2θ=10.50°), indicating an expanded interlayer spacing of 0.842 nm. This phenomenon can be attributed to the incorporation of EDA molecules, which induces an expansion of the interlayer spacing in the GO membrane. In comparison with the pristine GO and GE membranes, with the increase of PSSNa crosslinking amount, the diffraction peaks of the PGE-1, PGE-2, and PGE-3 membranes shift to even lower angles ($2\theta=9.48°$, 9.14°, and 8.58°, respectively), corresponding to interlayer spacings of 0.933 nm, 0.968 nm, and 1.031 nm, respectively. These findings indicate a further expansion of the interlayer spacing in the GO membrane, which facilitates reduced mass transfer resistance and significantly enhances water permeability. Furthermore, we performed XRD measurements on GO-based membranes in their wet states and systematically compared the variations in interlayer spacing between the dry and wet conditions. The results demonstrate that the swelling ratio of the interlayer spacing for the pristine GO membrane in the wet state is 57.2%. After EDA intercalation, the swelling ratio decreases to 41.9%. With the addition of PSSNa, the swelling behavior of the GO membrane is further limited. Collectively, these results suggest that the interlayer structural stability of the GO membrane is significantly improved under the synergistic effects of EDA and PSSNa.

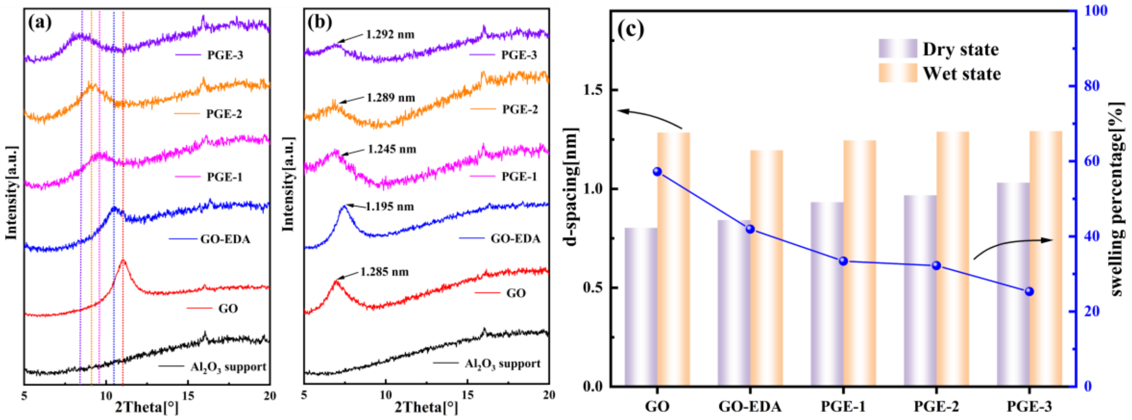

Fig. 9. XRD patterns of the GO-based membranes in the (a) dry and (b) wet states; (c) d-spacing and swelling percentage of GO-based membranes in dry and wet conditions

3.3 Pure water permeability of GO-based membranes

The pure water permeance of GO, GE, PGE-1, PGE-2, and PGE-3 was tested continuously for 4 h via a custom-built cross-flow filtration device, and the results are shown in Fig. 10. As the operation time increased, the permeation of GO, GE, PGE-1, PGE-2, PGE-3 membrane initially decreased before stabilizing. Pure water permeance in a stable state of GO, GE, PGE-1, PGE-2, and PGE-3 was 0.90, 1.46, 10.85, 4.59, and 4.12 LMH/bar. This result can be explained by the relatively loose structure and incomplete stacking of the GO nanosheets at the initial stage of filtration, which creates wide transport channels that facilitate the flow of water molecules [38]. However, as cross-flow time increases, the pressure gradually compresses this loose microstructure, reducing the available water transport pathways and decreasing permeance. The permeance of the GE membrane was found to be higher than that of the pristine GO membrane. This can be attributed to the increased interlayer distance resulting from the addition of EDA. Compared with pristine GO membrane, it can also be found that the permeability of PGE membranes (PGE-1, PGE-2, and PGE-3) was increased by 12.1, 5.1, and 4.6 times, respectively. The improvement in permeance can be attributed to the increase in interlayer distance of the PGE membranes caused by the introduction of EDA and PSSNa. Furthermore, the hydrophilic sulfonic acid groups, crosslinked within the interlayer of PGE membranes, could capture water molecules more effectively, thus creating additional pathways for water molecule transport. Consequently, the permeance of PGE membranes was greatly improved. The permeability of the PGE-1 membrane is higher than that of PGE-2 and PGE-3 membrane, which may be due to the following reasons. First, the thickness of PGE-2 and PGE-3 membrane increases, resulting in an increased mass transfer path and higher resistance for water molecules. Second, the excessive insertion of PSSNa could expand the interlayer spacing positively. Meanwhile, it also occupies a large amount of interlayer space to some extent, subsequently leading to a decrease in the permeation rate of the PGE-2 and PGE-3 membranes.

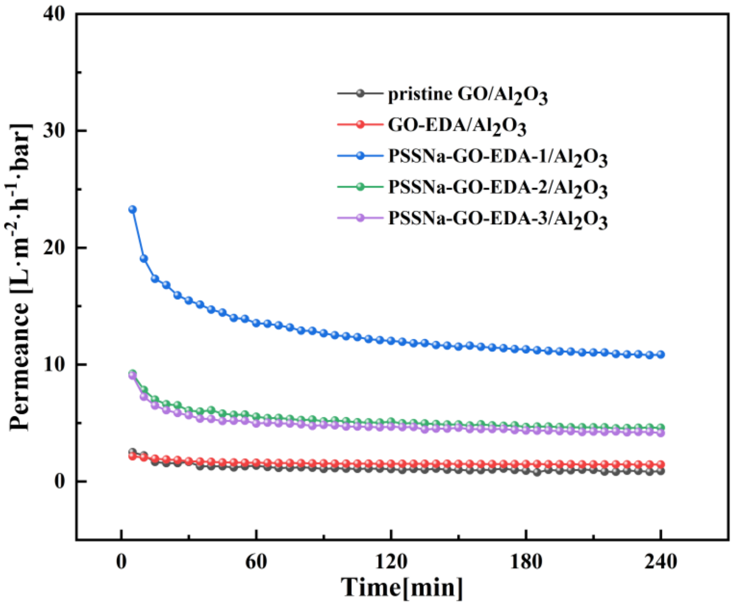

Fig. 10. Pure water permeance of pristine GO, GE, and PGE membranes

3.4 Desalination performance of GO-based membranes

To investigate the desalination performance of GO, GE, PGE-1, PGE- PGE-2, and PGE-3 membrane, the salt permeability and rejection were evaluated using four single-component salt solutions (Na_2SO_4, NaCl, $MgSO_4$, $MgCl_2$). Fig. 11 provides a visual representation of the results. The experimental results show that the rejection rates of the pristine GO membrane for Na_2SO_4, NaCl, $MgSO_4$, and $MgCl_2$ are 79.8%, 47.0%, 72.7%, and 23.2%, respectively, indicating a varied performance for different solutes. This finding is in agreement with those of previous studies[2, 12]. After crosslinking of the EDA, a decrease in salt rejection was observed, which agrees with the previous report[39]. The rejection rates of GO and GE membranes for the four single-component salt solutions are ranked as follows: Rejection rate (Na_2SO_4) > Rejection rate ($MgSO_4$) > Rejection rate (NaCl) > Rejection rate ($MgCl_2$), due to the synergistic effects of Donnan exclusion and size sieving[40].

In detail, based on the zeta potential results discussed above, GO and GE membranes are negatively charged. These membranes preferentially repel ions with the same charge as the GO membrane and attract ions with the opposite charge to the GO membrane, thereby ensuring the maintenance of charge neutrality throughout the entire system. This result can be attributed to the Donnan exclusion theory, as expressed in Eq. (3):

$$R = 1 - \frac{C_B^m}{C_B} = 1 - \left(\frac{|Z_B|C_B}{|Z_B|C_B^m + C_X^m}\right)^{|Z_B|/|Z_A|} \tag{3}$$

According to Eq. (3), the expected salt rejection order is R(Na_2SO_4) > R(NaCl) ≈R($MgSO_4$) > R($MgCl_2$). However, experimental results indicated that the rejection of $MgSO_4$ exceeded that of NaCl. This result can be ascribed to the varying hydration diameters of the respective ions, as evidenced by the hydration diameters of the ions: Mg^{2+} (8.6 Å) > SO_4^{2-} (7.6 Å) > Na^+ > Cl^- (6.6 Å)[41]. Thus, the hydration diameters of Mg^{2+} and SO_4^{2-} are larger compared to those of Na^+ and Cl^-, the latter of which are more readily rejected.

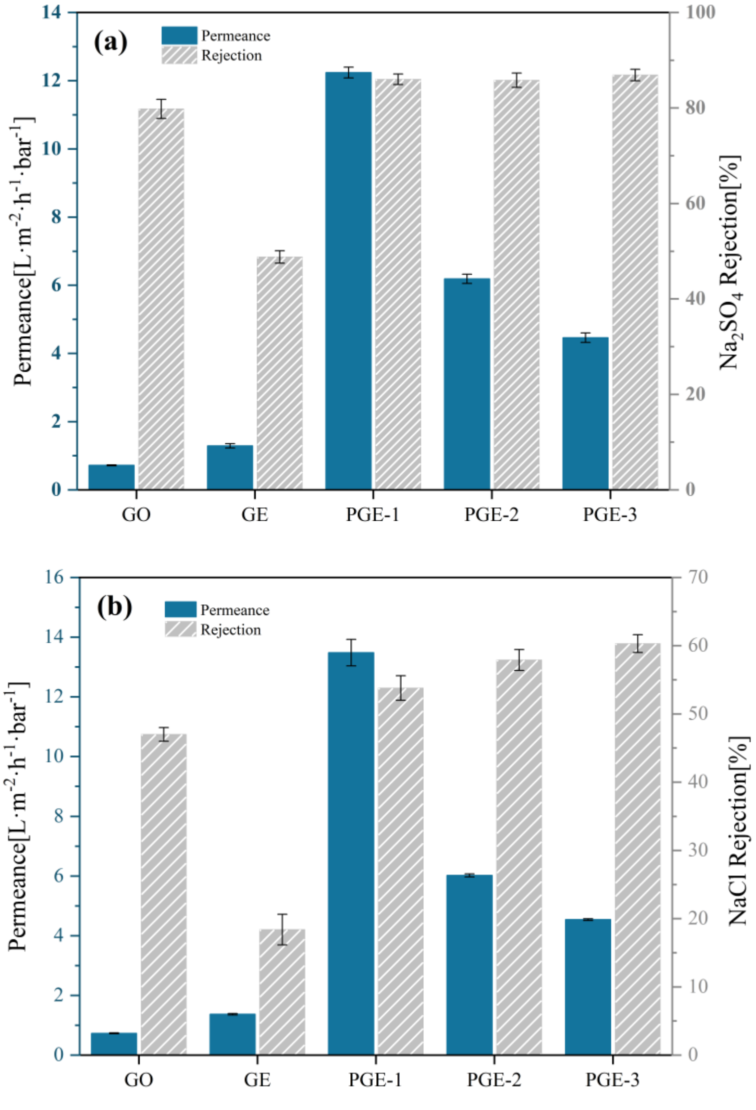

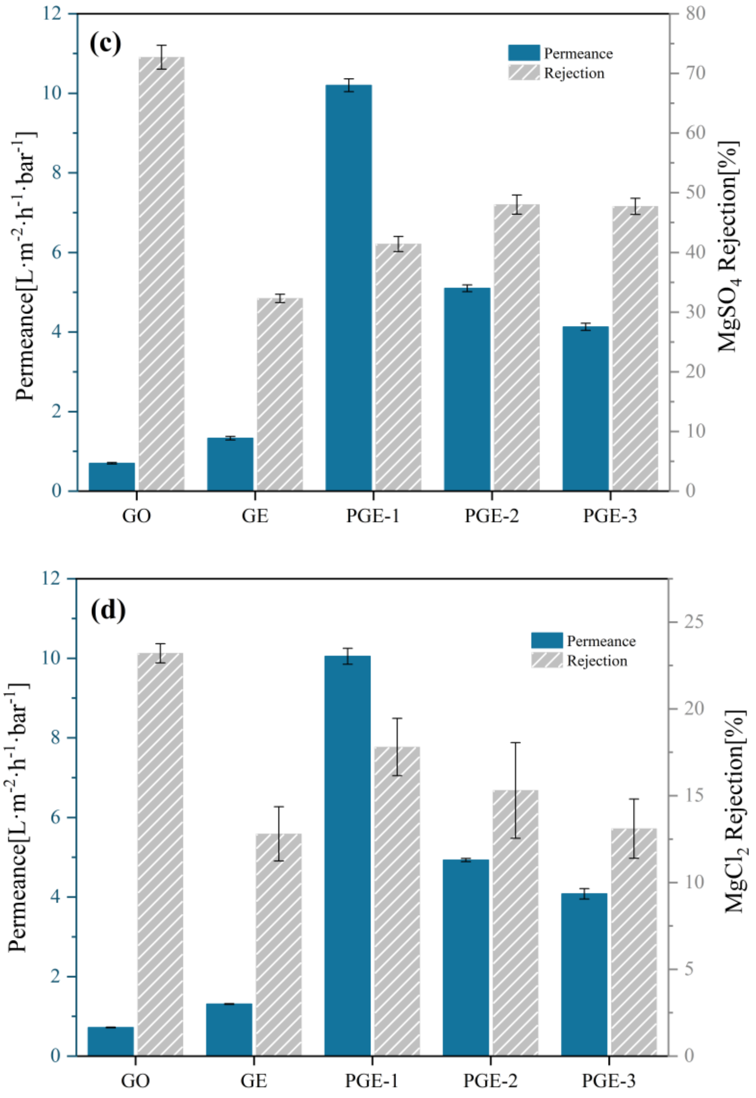

Fig. 11. Permeance and separation performance of GO and GE and PGE membranes towards four single-component salt solutions (a) Na_2SO_4, (b) NaCl, (c) $MgSO_4$, (d) $MgCl_2$

With regard to the PGE (PGE-1, PGE-2, PGE-3) membranes, the high permeability was sustained while a high salt rejection rate was also maintained, as shown in Fig. 11. Interestingly, the permeability of the salt solutions of the PGE membranes (PGE-1, PGE-2, PGE-3) was found to exceed that of the steady-state pure water of the PGE membranes (PGE-1, PGE-2, PGE-3). This was attributed to the fact that, during the testing of salt rejection, the permeate was collected immediately after stabilization for 40 min. Based on the osmotic pressure formula proposed by van't Hoff, osmotic pressure is directly proportional to the molar concentration of solute in the solution[42]. Salt solutions, which contain a high concentration of solutes, exhibit significantly higher osmotic pressures compared to pure water. During nanofiltration, the osmotic pressure of the solution generates a counteracting force opposing the driving force, thereby impeding the permeation of water molecules from the feed side through the membrane. In contrast, pure water, devoid of osmotic pressure, enables water molecules to pass through the nanofiltration membrane more efficiently under identical operating conditions, thus demonstrating superior permeability. Moreover, the viscosity of salt solutions is generally greater than that of pure water, increasing flow resistance and consequently resulting in lower permeability for salt solutions compared to pure water. The relationship is given by Eq. (4):

$$\Pi = \mathrm{icRT} \tag{4}$$

Where Π (Pa) is the osmotic pressure; i is the van't Hoff factor; c ($\mathrm{mol \cdot m^{-3}}$) is the molar concentration of the solute; R is the ideal gas constant, $R=8.314 \mathrm{J \cdot mol^{-1} \cdot K^{-1}}$; T (K) is the thermodynamic temperature.

After the same stabilization time, the slightly lower salt solution permeance compared to pure water permeance might be the consequence of higher osmotic pressure difference across the membrane and higher viscosity in the salt solution[43]. In addition, the rejection rates of PGE (PGE-1, PGE-2, PGE-3) membranes to Na_2SO_4 were 86.0%, 85.8%, and 86.9%, and those to NaCl were 53.8%, 57.9%, and 60.3%, respectively, which were all improved compared with those of GO and GE membranes.

Overall, the results demonstrate that PGE membranes (PGE-1, PGE-2, PGE-3) exhibit superior water permeability compared to most GO-based membranes while sustaining high salt rejection. This performance can primarily be attributed to two key factors, as illustrated in Fig. 12.

When a salt ion traverses a separation membrane to maintain electrical neutrality within the entire system, the salt ion is unable to permeate the membrane unassisted. Instead, it must form an electrically neutral ion-pair (i.e., in the form of a salt molecule) with a counter-ion (also known as the equilibrium ion), which together with the pores from the membrane, enables its permeation through the membrane. Similarly, ions cannot be retained by the membrane alone; in order to ensure the electrical neutrality of the system, the ion must be retained by the membrane in an ion pair with its counter-ion (the equilibrium ion)[44, 45]. Moreover, the transport of individual ions through nanometer or sub-nanometer membrane pores has been shown to be controlled by the intra-pore diffusion of ions[45, 46], which is influenced by interactions between the ions and the pore wall [47]. These interactions, typically electrostatic in nature, encompass both attractive and repulsive forces between the fixed charges on the membrane surface and the ions [48]. This underlines the significance of ion-pore interactions and intra-pore cation/anion modulation.

In contrast, the diffusion of ions in the lamellar channels of the PGE membrane is not only affected by the interactions of GO nanosheets on both sides of the nano-channels, but most importantly affected by the interactions between the ions and the PSSNa inserted in the interlayer. Consequently, the PGE membrane can achieve a high salt removal rate due to the introduction of poly(sodium 4-styrenesulfonate) polymer chains into the lamellar GO membrane, which leads to the formation of a hydrophilic nano-confined structure. The sulfonic groups within this structure then draw in ions through electrostatic induction, effectively confining them within the interlayer structure of the PGE membrane [49]. Thus, when salt ions traverse the membrane, they are affected by the aforementioned mechanism and are unable to pass through the membrane in the form of ion pairs with their equilibrium ions, thereby weakening their synergistic transport effect and achieving desalination. Additionally, the rejection of the PGE membranes to the four single-component salt solutions is also consistent with the $R(Na_2SO_4) > R(NaCl) > R(MgSO_4) > R(MgCl_2)$ order, which is in line with the Donnan effect theory. This indicates that the Donnan exclusion effect also contributes significantly

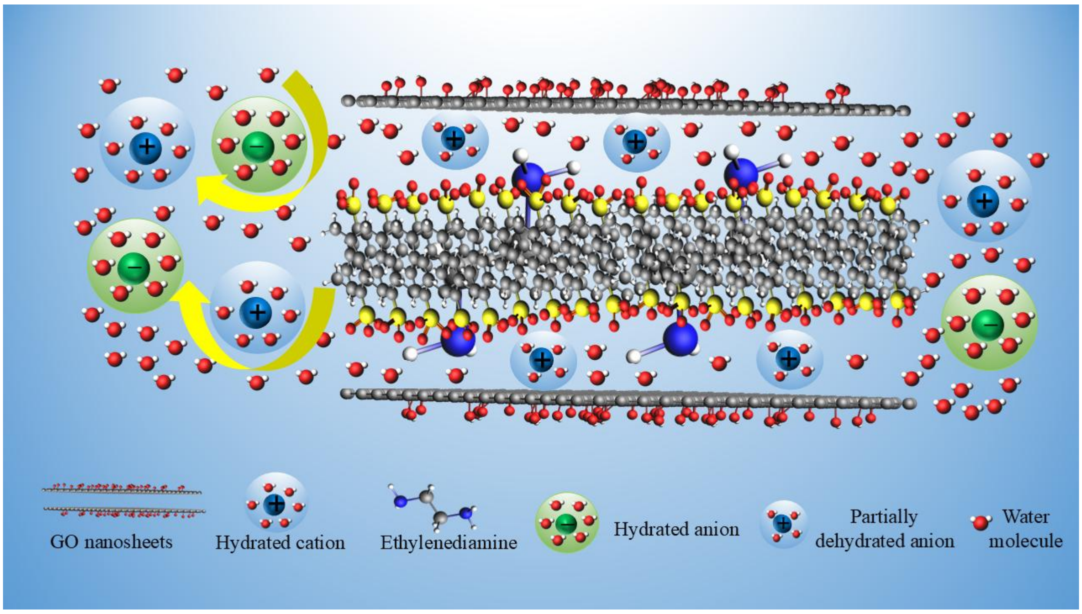

Fig. 12. Schematic illustration of separation mechanism through PGE membranes nanochannel.

3.5 Synergistic mechanism of EDA and PSSNa

Figure 13 and Table 1 show the comparison of the nanofiltration performance between GO-EDA, PSSNa-GO, and PSSNa-GO-EDA-1 membranes (GO: PSSNa=1:150). It was observed that the nanofiltration performance of GO-EDA and PSSNa-GO membranes was significantly inferior to that of PSSNa-GO-EDA-1 membranes. This suggests that the trade-off between selectivity and permeability can effectively be overcome only when EDA and PSSNa are simultaneously intercalated and crosslinked in GO membranes. The permeability of the membrane is enhanced by an order of magnitude (12 times higher than that of pristine GO membranes), while maintaining a high salt rejection rate. This improvement can be attributed to the synergistic effect of EDA and PSSNa, which not only further enhances the stability of GO membranes in water environments (Figure 9c), but also establishes hydrophilic nanoconfined microregions between GO layers by leveraging the unique properties of PSSNa. Such hydrophilic nanoconfined microregions facilitate the rapid and selective transport of water molecules and meanwhile improve the rejection of charged ions by GO membranes.

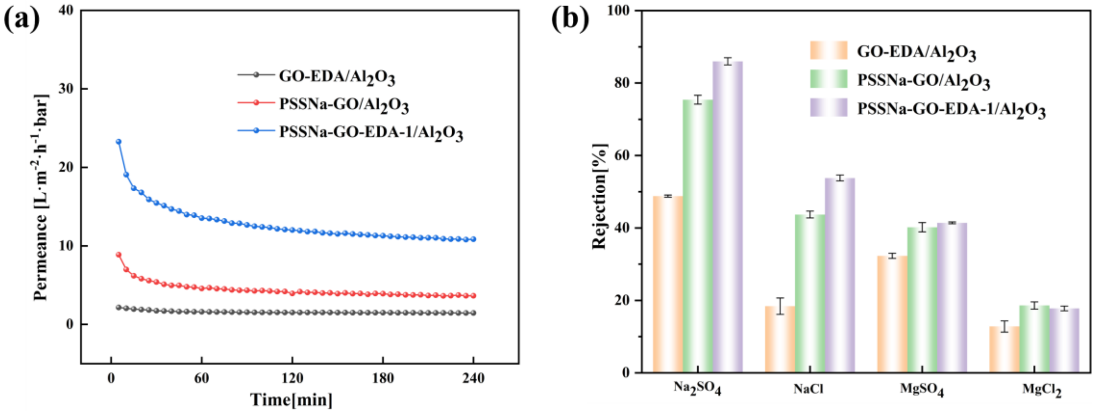

Fig. 13. Nanofiltration performance of GO-EDA, PSSNa-GO, PSSNa-GO-EDA-1 membrane (a) Pure water permeance (b) rejection performance for four salt solutions

Table 1 Nanofiltration performance of GO-EDA, PSSNa-GO, and PSSNa-GO-EDA-1 membrane

Membrane	***J*/** (LMH/bar)	***R*/%**			
		Na_2SO_4	NaCl	$MgSO_4$	$MgCl_2$
GO-EDA	1.46	48.8	18.4	32.3	12.8
PSSNa-GO-EDA-1	10.85	86.0	53.8	41.4	17.8
PSSNa-GO	3.65	75.4	43.7	40.2	18.6

3.6 Stability of GO-based membranes

The practical application of GO, GE, and PGE membranes is significantly hindered by their instability. Therefore, the application stability of the GO, GE, and PGE-1, PGE-2, PGE-3 membranes was tested by immersing them in pure water for varying periods of time. From Fig. 14, the permeance of the five GO-based membranes exhibits a slight decrease as the immersion time extends, whereas the rejection rates for the four salt solutions exhibit an increasing trend. After being immersed in water for 680 hours, the rejection rates of GO, GE, PGE-1, PGE-2, PGE-3 membranes to Na_2SO_4 reached 79.7%, 76.1%, 83.8%, 91.3% and 86.9%, respectively. The rejection rates of PGE membranes to four single-component salts exhibited minimal fluctuation within a defined range and slight change with the prolongation of immersion time. This finding indicates that the prepared membranes maintain remarkable stability in aqueous solutions. The reason may lie in the fact that the residual cation ions between layers produced cross-linking reactions with the GO nanosheets after many salt retention tests [11], increasing the density of the membrane.

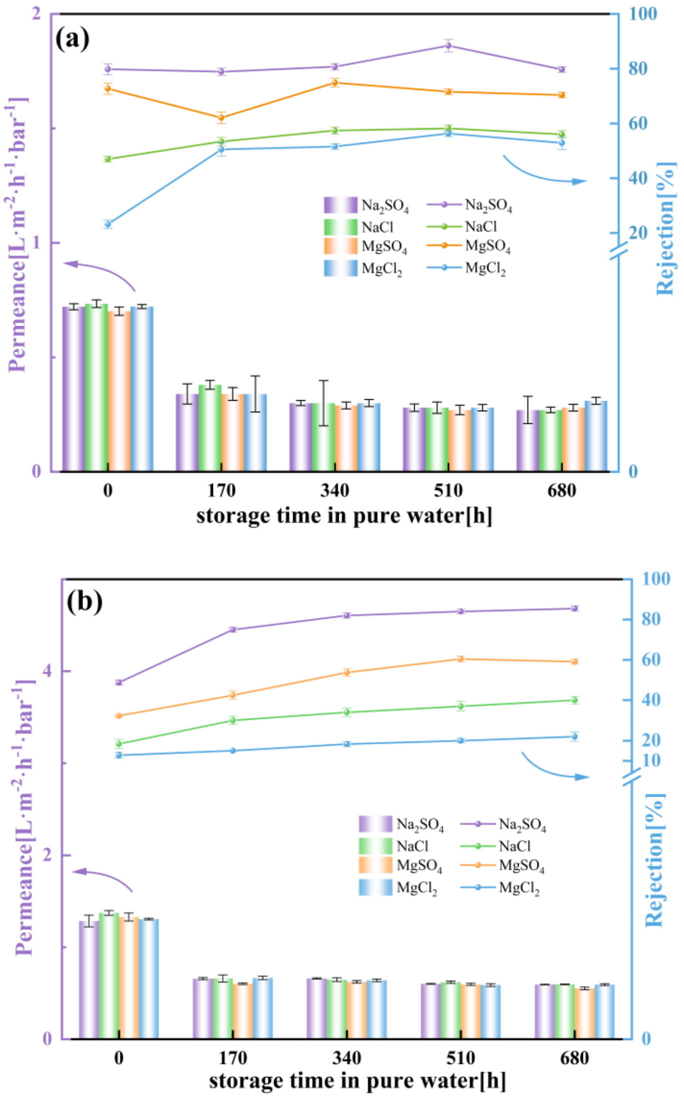

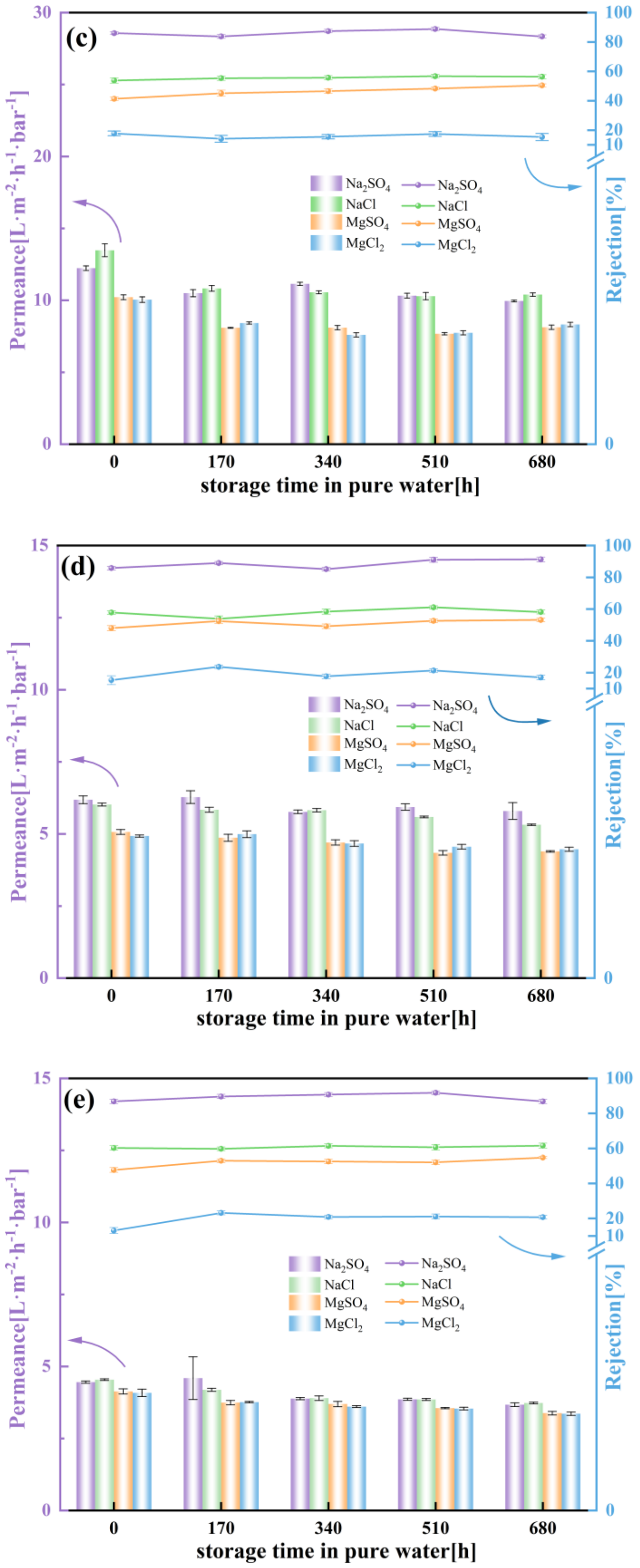

Fig. 14. Stability of GO and GE and PGE membranes (a) GO, (b) GE, (c) PGE-1, (d) PGE-2, (e) PGE-3

The mechanical stability of PGE-1 membrane is essential in industrial separation applications. Consequently, we also tested the mechanical stability of the PGE-1 membrane under higher operating pressure. With the escalation of the operating pressure, the permeability of the PGE-1 membrane approximates a linear increase, and the rejection rate of Na_2SO_4 also shows an ascending tendency (as shown in Fig. 15.). At 25 bar, the salt permeability reaches 295 $L \cdot m^{-2} \cdot h^{-1}$, with a Na_2SO_4 rejection rate of 95.2%. Under high pressure, the PGE-1 lamellar membrane still exhibits outstanding nanofiltration performance, thereby demonstrating its stable microstructure and high-pressure resistance. Under high-pressure circumstances, the performance of the membrane shows an upward trend. This trend can be analyzed by the dissolution-diffusion theory[50]. The salt permeance is determined by the difference in salt concentrations across the membrane. With the increase of pressure, the net pressure difference across the membrane rises, intensifying the concentration polarization of the membrane and consequently leading to elevated salt permeance. The salt rejection rate is dependent upon the concentration of salt in the permeate. If the rate of salt permeation exceeds that of water permeation, the salt rejection efficiency diminishes. Conversely, when the water permeation rate surpasses that of salt permeation, the salt rejection efficiency is enhanced.

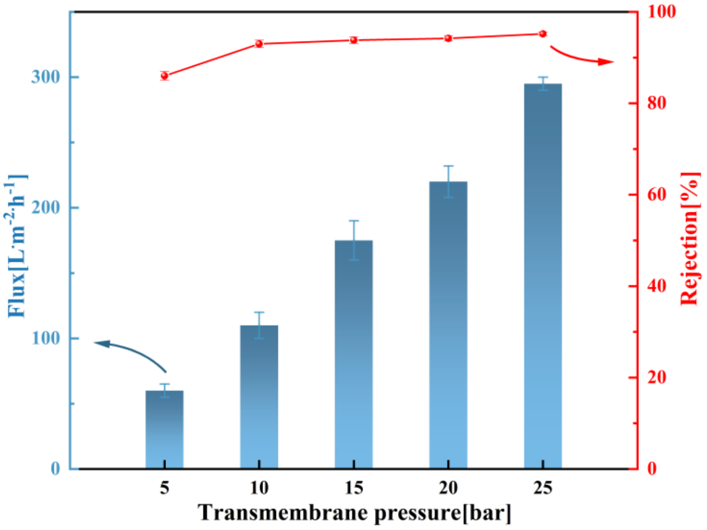

Fig. 15. Rejection of PGE-1 membrane towards 1 mM Na_2SO_4 solution under 5, 10, 15 ,20, 25 bar

Compared with the GO nanofiltration membranes reported in previous reports, the PGE-1 membrane in this paper still has highly competitive performance, as summarized in Table 1.

Table 2. Comparison of performance for PGE-1membrane with literature data for other membranes.

Membrane	Support	Feed condition	Testing condition	Water permeance (LMH/bar)	Rejection (%)	Ref.
Pristine GO	α-Al_2O_3	Na_2SO_4, $MgSO_4$ $MgCl_2$, NaCl	100 ppm 5 bar	3.68	72.6, 58.4 23.7, 45.8	[12]
RGO	PVDF	Na_2SO_4, NaCl $MgSO_4$, $MgCl_2$	20 mM 5 bar	3.3	~60,~ 30 ~20, ~40	[51]
RGO/sGO	PVDF	Na_2SO_4, NaCl $MgSO_4$, $MgCl_2$	1 mM 2 bar	3.78	86.3,60.5 40.9,35.7	[52]
RGO/g-C_3N_4	MCE	Na_2SO_4,NaCl	10 mM 1 bar	2.0	89.2, 67.5	[53]
GO-PEI	PAN	Na_2SO_4, $MgCl_2$, NaCl	10 mM 3 bar	4.0	30, 72 20	[54]
MoS_2/GO	PVDF	Na_2SO_4, NaCl $MgSO_4$, $MgCl_2$	1mM 2 bar	10.2	65.2, 43.2 24.3, 26.5	[55]
Commercial NF1	PS	Na_2SO_4, NaCl	/ 20 bar	3.45	98, 51	[56]
Commercial NF2	PAM	Na_2SO_4, NaCl	/ 20 bar	6.5	99, 44	[56]
Osmonics DK	/	NaCl	0.059~5.85 g/L /	3.05	22.0~75.6	[57]
Osmonics CK	/	NaCl	0.059~5.85 g/L /	2.42	45.5~77.7	[57]
PGE-1	Al_2O_3	Na_2SO_4, NaCl	1 mM 5 bar	10.85	86.0, 53.8	This work

4. Conclusion

In this paper, PSSNa-GO-EDA/Al_2O_3 membranes were successfully prepared by embedding PSSNa into amine-crosslinked GO interlayers using a pressure-driven deposition technique on tubular Al_2O_3 ultrafiltration membranes. The introduction of hydrophilic PSSNa polymer chains between GO interlayers not only enhances the regulation of interlayer spacing but also improves the chemical microenvironment. The introduced sulfonic acid groups significantly augment the hydrophilicity of the membrane, enhance its selective transportation of water molecules, and greatly boost its permeability. Furthermore, a nanoconfinement structure was fabricated in the laminar GO membranes by long-chain polystyrene sulfonic acid, which confines ions within the interlayer channels via the electrostatic attraction between sulfonic acid groups and ions. This breaks the correlation of anions and cations to suppress anion-cation co-transport, substantially improving the nanofiltration performance of the GO-based membranes. Of the GO, GE, and PGE membranes, the PGE-1 membrane maintains high salt rejection rates and increases water permeability by more than tenfold, and thus it demonstrates excellent separation performance and desalination stability. It also maintains favorable long-term stability, retaining high desalination performance even after being immersed in pure water for 680 hours. In conclusion, the construction of specialized domain-confined structures and targeted chemical microenvironments between the 2D membrane interlayers could be an effective strategy for achieving the ultrahigh nanofiltration performance of GO-based membranes and for applying them to real systems.

Acknowledgments

This study was supported by the National Natural Science Foundation of China (21490581) and China Petroleum & Chemical Corporation (317008-6).

References:

[1] P.J.J. Alvarez, C.K. Chan, M. Elimelech, N.J. Halas, D. Villagán, Emerging opportunities for nanotechnology to enhance water security, Nat. Nanotechnol. 13(8) (2018) 634-641. https://doi.org/10.1038/s41565-018-0203-2.

[2] Y.Y. Wu, C.F. Fu, Q. Huang, P.P. Zhang, P. Cui, J. Ran, J.L. Yang, T.W. Xu, 2D Heterostructured Nanofluidic Channels for Enhanced Desalination Performance of Graphene Oxide Membranes, ACS Nano 15(4) (2021) 7586-7595. https://doi.org/10.1021/acsnano.1c01105.

[3] R.P. Lively, D.S. Sholl, From water to organics in membrane separations, Nature Materials 16(3) (2017) 276-279. https://doi.org/10.1038/nmat4860.

[4] B. Sapkota, W.T. Liang, A. VahidMohammadi, R. Karnik, A. Noy, M. Wanunu, High permeability sub-nanometre sieve composite MoS_2 membranes, Nat. Commun. 11(1) (2020) 9.

https://doi.org/10.1038/s41467-020-16577-y.

[5] D.S. Sholl, R.P. Lively, Seven chemical separations to change the world, Nature 532(7600) (2016) 435-437. https://doi.org/10.1038/532435a.

[6] J. Shen, G.P. Liu, Y. Han, W.Q. Jin, Artificial channels for confined mass transport at the sub-nanometre scale, Nat. Rev. Mater. 6(4) (2021) 294-312. https://doi.org/10.1038/s41578-020-00268-7.

[7] Z.D. Xiong, L.H. Dai, Y.X. Wang, K. Qu, Y.S. Xia, L.F. Lei, K. Huang, Z. Xu, Two-dimensional sub-nanometer confinement channels enabled by functional carbon dots for ultra-permeable alcohol dehydration, J. Membr. Sci. 644 (2022) 10. https://doi.org/10.1016/j.memsci.2021.120069.

[8] L.Y. Zhang, M.C. Zhang, G.P. Liu, W.Q. Jin, X.Y. Li, Fungal Cell Wall-Graphene Oxide Microcomposite Membrane for Organic Solvent Nanofiltration, Adv. Funct. Mater. 31(23) (2021) 9. https://doi.org/10.1002/adfm.202100110.

[9] W.H. Zhang, M.J. Yin, Q. Zhao, C.G. Jin, N.X. Wang, S.L. Ji, C.L. Ritt, M. Elimelech, Q.F. An, Graphene oxide membranes with stable porous structure for ultrafast water transport, Nat. Nanotechnol. 16(3) (2021) 337-+. https://doi.org/10.1038/s41565-020-00833-9.

[10] G. Romanos, L.M. Pastrana-Martínez, T. Tsoufis, C. Athanasekou, E. Galata, F. Katsaros, E. Favvas, K.G. Beltsios, E. Siranidi, P. Falaras, V. Psycharis, A.M.T. Silva, A facile approach for the development of fine-tuned self-standing graphene oxide membranes and their gas and vapor separation performance, J. Membr. Sci. 493 (2015) 734-747. https://doi.org/10.1016/j.memsci.2015.07.034.

[11] C.N. Yeh, K. Raidongia, J.J. Shao, Q.H. Yang, J.X. Huang, On the origin of the stability of graphene oxide membranes in water, Nature Chemistry 7(2) (2015) 166-170. https://doi.org/10.1038/nchem.2145.

[12] B.Q. Yuan, M.X. Wang, B. Wang, F.L. Yang, X. Quan, C.Y.Y. Tang, Y.C. Dong, Cross-linked Graphene Oxide Framework Membranes with Robust Nano-Channels for Enhanced Sieving Ability, Environ. Sci. Technol. 54(23) (2020) 15442-15453. https://doi.org/10.1021/acs.est.0c05387.

[13] S. Wang, S.S. Liang, L. Chen, H.P. Fang, Realizing ultrahigh nanofiltration performance based on small flake reduced graphene oxide membranes, Desalination 528 (2022) 10. https://doi.org/10.1016/j.desal.2022.115601.

[14] S.X. Zheng, Q.S. Tu, J.J. Urban, S.F. Li, B.X. Mi, Swelling of Graphene Oxide Membranes in Aqueous Solution: Characterization of Interlayer Spacing and Insight into Water Transport Mechanisms, Acs Nano 11(6) (2017) 6440-6450. https://doi.org/10.1021/acsnano.7b02999.

[15] P.C. Su, F. Wang, Z.J. Li, C.Y. Tang, W.B. Li, Graphene oxide membranes: controlling their transport pathways, J. Mater. Chem. A 8(31) (2020) 15319-15340. https://doi.org/10.1039/d0ta02249g.

[16] J. Wang, H.J. Zhou, S.Z. Li, L. Wang, Selective Ion Transport in Two-Dimensional Lamellar Nanochannel Membranes, Angew. Chem.-Int. Edit. 62(19) (2023) 22. https://doi.org/10.1002/anie.202218321.

[17] J. Abraham, K.S. Vasu, C.D. Williams, K. Gopinadhan, Y. Su, C.T. Cherian, J. Dix, E. Prestat, S.J. Haigh, I.V. Grigorieva, P. Carbone, A.K. Geim, R.R. Nair, Tunable sieving of ions

using graphene oxide membranes, Nature Nanotechnology 12(6) (2017) 546-+. https://doi.org/10.1038/nnano.2017.21.

[18] N.K. Khanzada, S. Rehman, S.Y. Leu, A.K. An, Evaluation of anti -bacterial adhesion performance of polydopamine cross-linked graphene oxide RO membrane via in situ optical coherence tomography, Desalination 479 (2020) 10. https://doi.org/10.1016/j.desal.2020.114339.

[19] S. Rajesh, A.B. Bose, Development of Graphene Oxide Framework Membranes via the "from" and "to" Cross-Linking Approach for Ion-Selective Separations, ACS Appl. Mater. Interfaces 11(31) (2019) 27706-27716. https://doi.org/10.1021/acsami.9b05465.

[20] I. Chandio, F.A. Janjhi, A.A. Memon, S. Memon, Z. Ali, K.H. Thebo, A.A.A. Pirzado, A.A. Hakro, W.S. Khan, Ultrafast ionic and molecular sieving through graphene oxide based composite membranes, Desalination 500 (2021) 9. https://doi.org/10.1016/j.desal.2020.114848.

[21] F.A. Janjhi, I. Chandio, A.A. Memon, Z. Ahmed, K.H. Thebo, A.A.A. Pirzado, A.A. Hakro, M. Iqbal, Functionalized graphene oxide based membranes for ultrafast molecular separation, Sep. Purif. Technol. 274 (2021) 8. https://doi.org/10.1016/j.seppur.2020.117969.

[22] E. Halakoo, X.S. Feng, Layer-by-layer assembled membranes from graphene oxide and polyethyleneimine for ethanol and isopropanol dehydration, Chem. Eng. Sci. 216 (2020) 16. https://doi.org/10.1016/j.ces.2020.115488.

[23] M.C. Zhang, Y.Y. Mao, G.Z. Liu, G.P. Liu, Y.Q. Fan, W.Q. Jin, Molecular Bridges Stabilize Graphene Oxide Membranes in Water, Angew. Chem.-Int. Edit. 59(4) (2020) 1689-1695. https://doi.org/10.1002/anie.201913010.

[24] F.C. Jia, L. Yang, Z.H. Li, L.Y. Sun, D.H. Yu, Y. Song, Y.X. Wang, L.J. Huang, J.G. Tang, Graphene oxide/sodium alginate nanofiltration membrane with double cross-linked structure for high-performance in dye separation, J. Mater. Sci. 58(15) (2023) 6618-6631. https://doi.org/10.1007/s10853-023-08433-3.

[25] J. Yu, Y. He, Y.Q. Wang, S.S. Li, S.T. Tian, Ethylenediamine-oxidized sodium alginate hydrogel cross-linked graphene oxide nanofiltration membrane with self-healing property for efficient dye separation, Journal of Membrane Science 670 (2023) 12. https://doi.org/10.1016/j.memsci.2023.121366.

[26] D.L. Xu, H. Liang, X.W. Zhu, L. Yang, X.S. Luo, Y.Q. Guo, Y.T. Liu, L.M. Bai, G.B. Li, X.B. Tang, Metal-polyphenol dual crosslinked graphene oxide membrane for desalination of textile wastewater, Desalination 487 (2020) 11. https://doi.org/10.1016/j.desal.2020.114503.

[27] L.P. Shao, Y. Li, F.S. Pan, Z.M. Zhang, S.W. Liang, Y.T. Wang, J.Y. Zou, Z.Y. Jiang, Graphene oxide membranes tuned by metal-phytic acid coordination complex for butanol dehydration, Journal of Membrane Science 638 (2021) 8. https://doi.org/10.1016/j.memsci.2021.119736.

[28] L.H. Dai, Z.D. Xiong, W.Y. Xu, K. Qu, Y.X. Wang, S.Y. Gu, H.Y. Cao, Y. Yu, L.F. Lei, S.Y. Li, K. Huang, X.H. Guo, Z. Xu, Two-dimensional confined channels with high-density hydrophilic microregions for enhanced selective water transport, Journal of Membrane Science 671 (2023) 8. https://doi.org/10.1016/j.memsci.2023.121398.

[29] R.Q. Cao, S.Y. Shi, H.B. Cao, Y.J. Li, F. Duan, Y.P. Li, Surface composite modification of anion exchange membrane by electrodeposition and self-polymerization for improved

antifouling performance, Colloid Surf. A-Physicochem. Eng. Asp. 648 (2022) 9. https://doi.org/10.1016/j.colsurfa.2022.129402.

[30] K. Zahri, K.C. Wong, P.S. Goh, A.F. Ismail, Graphene oxide/polysulfone hollow fiber mixed matrix membranes for gas separation, RSC Adv. 6(92) (2016) 89130-89139. https://doi.org/10.1039/c6ra16820e.

[31] S.J. Xia, M. Ni, T.R. Zhu, Y. Zhao, N.N. Li, Ultrathin graphene oxide nanosheet membranes with various d-spacing assembled using the pressure-assisted filtration method for removing natural organic matter, Desalination 371 (2015) 78-87. https://doi.org/10.1016/j.desal.2015.06.005.

[32] Y.L. Qian, X.L. Zhang, C.Y. Liu, C. Zhou, A.S. Huang, Tuning interlayer spacing of graphene oxide membranes with enhanced desalination performance, Desalination 460 (2019) 56-63. https://doi.org/10.1016/j.desal.2019.03.009.

[33] W.S. Hung, C.H. Tsou, M. De Guzman, Q.F. An, Y.L. Liu, Y.M. Zhang, C.C. Hu, K.R. Lee, J.Y. Lai, Cross-Linking with Diamine Monomers To Prepare Composite Graphene Oxide-Framework Membranes with Varying d-Spacing, Chemistry of Materials 26(9) (2014) 2983-2990. https://doi.org/10.1021/cm5007873.

[34] Z. Lu, Y. Wu, L. Ding, Y.Y. Wei, H.H. Wang, A Lamellar MXene (Ti_3C_2Tx)/PSS Composite Membrane for Fast and Selective Lithium-Ion Separation, Angew. Chem.-Int. Edit. 60(41) (2021) 22265-22269. https://doi.org/10.1002/anie.202108801.

[35] F. Liang, H.Y. Wang, G.Z. Liu, J. Zhao, W.Q. Jin, Designing highly selective and stable water transport channel through graphene oxide membranes functionalized with polyhedral oligomeric silsesquioxane for ethanol dehydration, J. Membr. Sci. 638 (2021) 11. https://doi.org/10.1016/j.memsci.2021.119675.

[36] S. Liu, G.Y. Zhou, K.C. Guan, X. Chen, Z.Y. Chu, G.P. Liu, W.Q. Jin, Dehydration of C_2-C_4 alcohol/water mixtures via electrostatically enhanced graphene oxide laminar membranes, Aiche Journal 67(6) (2021) 11. https://doi.org/10.1002/aic.17170.

[37] K.H. Thebo, X.T. Qian, Q. Zhang, L. Chen, H.M. Cheng, W.C. Ren, Highly stable graphene-oxide-based membranes with superior permeability, Nature Communications 9 (2018) 8. https://doi.org/10.1038/s41467-018-03919-0.

[38] J.Y. Chong, B. Wang, K. Li, Water transport through graphene oxide membranes: the roles of driving forces, Chemical Communications 54(20) (2018) 2554-2557. https://doi.org/10.1039/c7cc09120f.

[39] Y. Zhang, S. Zhang, T.S. Chung, Nanometric Graphene Oxide Framework Membranes with Enhanced Heavy Metal Removal via Nanofiltration, Environ. Sci. Technol. 49(16) (2015) 10235-10242. https://doi.org/10.1021/acs.est.5b02086.

[40] S.F. Wang, L.X. Yang, G.W. He, B.B. Shi, Y.F. Li, H. Wu, R.N. Zhang, S. Nunes, Z.Y. Jiang, Two-dimensional nanochannel membranes for molecular and ionic separations, Chem. Soc. Rev. 49(4) (2020) 1071-1089. https://doi.org/10.1039/c9cs00751b.

[41] I. Shefer, O.P. Haim, R. Epsztein, Limited ion-ion selectivity of salt-rejecting membranes due to enthalpy-entropy compensation, Desalination 541 (2022) 10. https://doi.org/10.1016/j.desal.2022.116041.

[42] J.H. Vanthoff, The role of osmotic pressure in the analogy between solutions and gases,

Journal of Membrane Science 100(1) (1995) 39-44. https://doi.org/10.1016/0376-7388(94)00232-n.

[43] M.C. Zhang, J.J. Sun, Y.Y. Mao, G.P. Liu, W.Q. Jin, Effect of substrate on formation and nanofiltration performance of graphene oxide membranes, Journal of Membrane Science 574 (2019) 196-204. https://doi.org/10.1016/j.memsci.2018.12.071.

[44] I.V. Khavrutskii, A.A. Gorfe, B.Z. Lu, J.A. McCammon, Free Energy for the Permeation of Na^+ and Cl^- Ions and Their Ion-Pair through a Zwitterionic Dimyristoyl Phosphatidylcholine Lipid Bilayer by Umbrella Integration with Harmonic Fourier Beads, J. Am. Chem. Soc. 131(5) (2009) 1706-1716. https://doi.org/10.1021/ja8081704.

[45] X.C. Zhou, Z.X. Wang, R. Epsztein, C. Zhan, W.L. Li, J.D. Fortner, T.A. Pham, J.H. Kim, M. Elimelech, Intrapore energy barriers govern ion transport and selectivity of desalination membranes, Sci. Adv. 6(48) (2020) 9. https://doi.org/10.1126/sciadv.abd9045.

[46] S.B. Sigurdardottir, R.M. DuChanois, R. Epsztein, M. Pinelo, M. Elimelech, Energy barriers to anion transport in polyelectrolyte multilayer nanofiltration membranes: Role of intra-pore diffusion, J. Membr. Sci. 603 (2020) 9.

[47] R. Epsztein, R.M. DuChanois, C.L. Ritt, A. Noy, M. Elimelech, Towards single-species selectivity of membranes with subnanometre pores, Nature Nanotechnology 15(6) (2020) 426-436. https://doi.org/10.1038/s41565-020-0713-6.

[48] C.H. Lu, C.Z. Hu, Z.B. Chen, P.Y. Wang, F. Feng, G.Z. He, F.Y. Wang, Y.Y. Zhang, J.Z. Liu, X.W. Zhang, J.H. Qu, Dehydration-enhanced ion-pore interactions dominate anion transport and selectivity in nanochannels, Sci. Adv. 9(27) (2023) 13. https://doi.org/10.1126/sciadv.adf8412.

[49] H.G. Zhang, J.J. Xing, G.L. Wei, X. Wang, S. Chen, X. Quan, Electrostatic-induced ion-confined partitioning in graphene nanolaminate membrane for breaking anion-cation co-transport to enhance desalination, Nature Communications 15(1) (2024) 13. https://doi.org/10.1038/s41467-024-48681-8.

[50] K. Popper, R.L. Merson, W.M. Camirand, Desalination by osmosis--reverse osmosis couple, Science (New York, N.Y.) 159(3821) (1968) 1364-5. https://doi.org/10.1126/science.159.3821.1364.

[51] Y. Han, Z. Xu, C. Gao, Ultrathin Graphene Nanofiltration Membrane for Water Purification, Advanced Functional Materials 23(29) (2013) 3693-3700. https://doi.org/10.1002/adfm.201202601.

[52] P. Zhang, J.L. Gong, G.M. Zeng, B. Song, S.Y. Fang, M. Zhang, H.Y. Liu, S.Y. Huan, P. Peng, Q.Y. Niu, D.B. Wang, J. Ye, Enhanced permeability of rGO/S-GO layered membranes with tunable interstructure for effective rejection of salts and dyes, Sep. Purif. Technol. 220 (2019) 309-319. https://doi.org/10.1016/j.seppur.2019.03.041.

[53] Z.J. Li, Y.C. Xing, X.Y. Fan, L.G. Lin, A. Meng, Q.D. Li, rGO/protonated g-C_3N_4 hybrid membranes fabricated by photocatalytic
reduction for the enhanced water desalination, Desalination 443 (2018) 130-136. https://doi.org/10.1016/j.desal.2018.05.019.

[54] Y. Liu, S.X. Zheng, P. Gu, A.J. Ng, M.N. Wang, Y.Y. Wei, J.J. Urban, B.X. Mi, Graphene-polyelectrolyte multilayer membranes with tunable structure and internal charge, Carbon 160

(2020) 219-227. https://doi.org/10.1016/j.carbon.2019.12.092.

[55] P. Zhang, J.L. Gong, G.M. Zeng, B. Song, W.C. Cao, H.Y. Liu, S.Y. Huan, P. Peng, Novel “loose” GO/MoS_2 composites membranes with enhanced permeability for effective salts and dyes rejection at low pressure, J. Membr. Sci. 574 (2019) 112-123. https://doi.org/10.1016/j.memsci.2018.12.046.

[56] N.K. Zaman, R. Rohani, A.W. Mohammad, J.M. Jahim, New polymeric membrane nanofiltration for succinate recovery: a comparative study, J. Polym. Res. 24(11) (2017) 15. https://doi.org/10.1007/s10965-017-1359-4.

[57] A.W. Mohammad, R.K. Basha, C.P. Leo, Nanofiltration of glucose solution containing salts: Effects of membrane characteristics, organic component and salts on retention, J. Food Eng. 97(4) (2010) 510-518. https://doi.org/10.1016/j.jfoodeng.2009.11.010.